

# Evaluation of Transformer Leakage Inductance Using Magnetic Image Method

Angshuman Sharma, *Student Member, IEEE*, and Jonathan W. Kimball, *Senior Member, IEEE*

Department of Electrical and Computer Engineering, Missouri University of Science and Technology, Rolla, MO 65401, USA

Leakage inductance is a critical design element of a transformer in a galvanically isolated power converter. For multi-objective optimization-based designs of power converters, analytical leakage inductance models that are computationally efficient and accurate are preferred over the Finite Element Methods (FEM). In this paper, three new analytical models are proposed—Triple-2D, Double-2D, and Single-2D—that are formulated using the magnetic image method. These 2D models are used to calculate the leakage inductance of a partially filled shell-type transformer having a circular center leg, and the resulting errors are less than 1.25 % for each model when compared to the 3D FEM simulated value of the leakage inductance. Additionally, three different conductor models are considered, and their relative accuracies and computational efficiencies are investigated. Further, a variable inductance transformer (VIT) is designed, whose leakage inductance can be modified by moving one of the windings vertically along the central core leg. The analytically evaluated variable leakage inductances of the VIT are in good agreement with the 3D FEM simulated and experimentally measured values.

*Index Terms*—Galvanically isolated power converter, image method, leakage inductance, shell-type transformer.

## I. INTRODUCTION

LEAKAGE INDUCTANCE is a key design property of a power electronic transformer. For some galvanically isolated power converter topologies, like the flyback [1], [2] and forward [3], a negligible leakage inductance can help in minimizing the power loss in the converter. For other topologies, like the half-bridge and full-bridge, a substantial leakage inductance can help in replacing the series inductor to reduce the cost of components and improve the power density of the converter [4]–[10]. In recent years, there has been a growing demand for such transformers with integrated magnetics that allow designers to utilize the leakage inductance purposefully for the operation of a power electronic converter. In a phase-shifted dual active bridge converter, the leakage inductance can provide the desired phase-shift between the primary and secondary bridges to cause power flow [4], [5]. In a resonant converter, the leakage inductance can participate in establishing the resonant frequency and voltage gain of the converter [6]–[8]. The leakage inductance can also help in ensuring zero-voltage switching in isolated power converters to meet the high-efficiency requirements [9]. Therefore, an accurate estimation of the transformer leakage inductance is critical for the design and operation of any galvanically isolated power converter.

Leakage inductance can be calculated from the leakage energy stored inside and outside the volume of the transformer when perfectly opposed magnetomotive forces (MMFs) are applied to the two windings of the transformer [11], i.e.,  $N_1 I_1 = N_2 I_2$ , where  $N_1$  and  $N_2$  are the number of primary and secondary turns, and  $I_1$  and  $I_2$  are the primary and secondary currents, respectively. Calculation of leakage inductance is inherently a three-dimensional (3D) problem. Finite Element Methods (FEM) can calculate the leakage inductance quite accurately, but at the expense of high computational effort, especially for 3D FEM [11], [12]. Reluctance network models were proposed in [13], [14], but they lack the desired accuracy.

For multi-objective optimization-based designs of isolated converters, analytical models having a lower computational effort with no significant loss in accuracy are desired [15], [16].

This retriggered the development of several 1D and 2D models, which calculate the total leakage inductance from the leakage inductance per unit length evaluated across a single 2D (Single-2D models) plane inside the winding window (IW plane) of the transformer [16]–[26]. Leakage inductance per unit length across a plane is proportional to the magnetic energy density across it. While the 2D models assume that the magnetic energy density varies along both the width and height of the window, the 1D models simplify the mathematics by assuming that the magnetic energy density is constant throughout the window height. This central assumption limits the scope of 1D models to designs where the winding height is comparable to the window height to avoid any calculation error due to the fringing fields across the edges of the conductors [16]. Hence, 2D models are more accurate, although 1D models are computationally more efficient.

Both 1D and Single-2D models assume that the leakage inductance per unit length calculated across the IW plane is consistent throughout the entire third dimension, which is usually the mean length of turn (MLT) of the windings. The highly-permeable ( $\mu_r \gg 1000$ ) core of a medium or high-frequency transformer acts as a reflective medium for the magnetic field intensities [27]. The finite IW plane across which the leakage inductance per unit length is calculated is bounded by the core on four sides, whereas the semi-infinite plane outside the window (OW plane) is bounded by the core on one side only. As such, the IW plane includes the contributions from an infinite series of images, while the OW plane includes the contribution from a single image only. Therefore, the leakage inductance per unit length calculated across the IW plane is naturally higher than that across the OW plane. This difference can introduce a substantial error in Single-2D models.

Double-2D models were introduced recently [11], [28], [29], where the leakage inductance per unit length is evaluated across two planes—IW plane and OW plane—hence the name “Double-2D”. The total leakage inductance is obtained by adding the product of the two leakage inductances per unit length and their respective partial winding lengths, called leakage lengths. The partial leakage lengths act as scaling

factors for the calculated leakage inductances per unit length. The overall accuracy of the model depends on the accurate evaluation of the two leakage inductances per unit length as well as the two partial leakage lengths. The Double-2D models are very promising because they can accurately calculate the leakage inductance even when the winding height is significantly smaller than the window height [28].

The Double-2D model proposed in [28] identified a transition (TR) region where the IW region merges into the OW region, but the TR region was not modeled. The TR region is of chief interest because across this region, the core yoke shrinks in size. So, the leakage inductance per unit length across the TR plane lies between those across the IW and OW planes. A shell-type transformer has four TR regions, whereas a core-type transformer has two. Accurate identification and modeling of the TR region are found to be critical, especially for shell-type transformers with partially filled windows. Moreover, analysis of the TR region can lead to the introduction of more effective leakage inductance models.

Partial leakage lengths are functions of the magnetic energy distributions across the respective planes, and hence must be evaluated from the energy-weighted radii, especially for concentric windings wound around a circular core leg [28]. Techniques to calculate the energy-weighted partial leakage lengths for IW and OW regions were proposed for the Double-2D model in [13], [28]. However, the IW and OW regions were selected intuitively without any justification, which can affect the accuracy of the partial leakage lengths, and consequently the total leakage inductance. Proper classification of the IW and OW regions is, therefore, missing in the literature.

Many 2D models use the magnetic image method to calculate the leakage inductance per unit length across a plane [11], [19]–[21], [29]. According to the image method, the layers of images that should be considered for an accurate evaluation of leakage inductance per unit length across the IW plane are infinite, which is practically not possible. Usually, a finite number of image layers that optimizes both accuracy and computational efficiency is considered [11]. Gomez [19] and Lambert [21] presented plots showing the number of image layers versus accuracy. However, Gomez assumed an incorrect direction of current for the image conductors, whereas Lambert assumed the MLT of the windings as the leakage length.

The geometry of the conductors assumed for evaluating the leakage inductance also influences the accuracy and computational efficiency of the image method [11]. A round conductor is difficult to model because of its distinct formulations for calculating the magnetic field intensities inside and outside its cross-sectional area. Windings comprising numerous round conductors further aggravate the problem. Although the popular choice is to assume a layer of round conductors or Litz wire as a rectangular foil, the resulting loss in accuracy or gain in computational efficiency is not known. Besides, assuming a foil thickness equal to the diameter of a round conductor only intensifies the error.

This paper introduces a Triple-2D model for calculating the leakage inductance of a transformer: besides the IW and OW planes, the leakage inductance per unit length is analytically evaluated across a third plane inside the transition region (TR plane) using the magnetic image method. IW, OW, and TR regions are identified, and a method to accurately calculate the

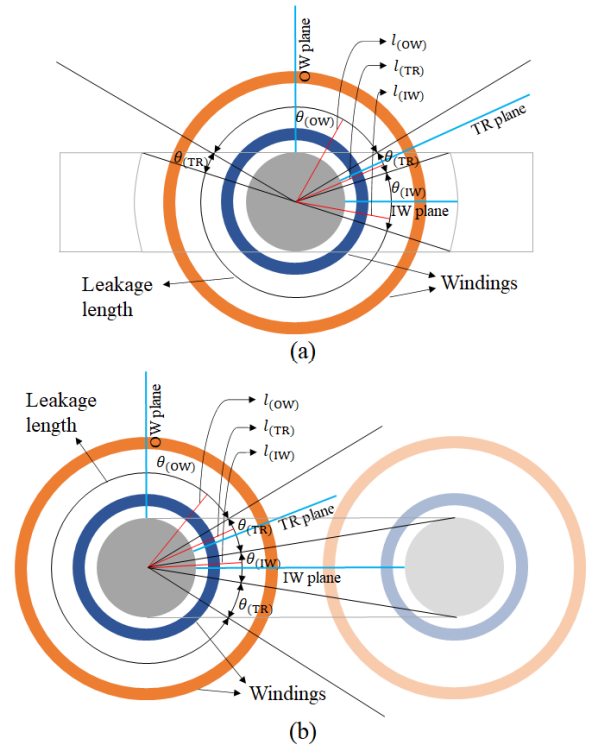


Fig. 1. Proposed Triple-2D model for: (a) shell-type transformer, and (b) core-type transformer.

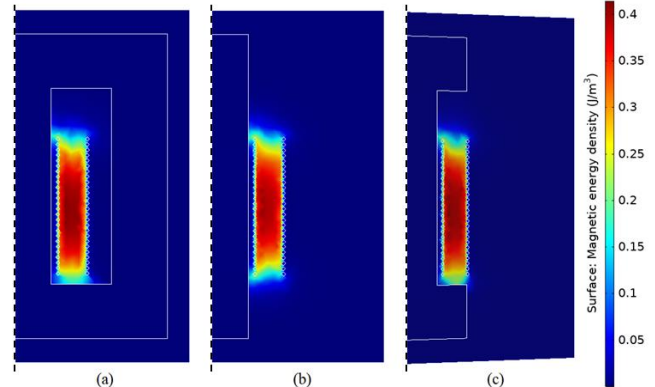


Fig. 2. Magnetic energy densities obtained from the 3D FEM model: (a) IW plane, (b) OW plane, and (c) TR plane.

energy-weighted partial leakage lengths is proposed. The Triple-2D model is first reduced to a new Double-2D model, and further to a unique Single-2D model to improve the computational efficiency. These 2D models are centered around the investigation of the TR region, as discussed above. Further, three different conductor models are analyzed using the proposed 2D models. The shell-type transformer assumed for validating the hypotheses has a partially filled winding window: the circular central core leg is wound with round conductors up to a height that is significantly smaller than the window height. By moving one of the windings vertically along the core leg, the leakage inductance of the transformer can be modified, thus resulting in a variable inductance transformer (VIT) [30]. The leakage inductances of the VIT are analytically evaluated and plotted for various positions of the winding. Finally, all analytical results are validated using 3D FEM simulations and experimental measurements obtained from a transformer prototype.

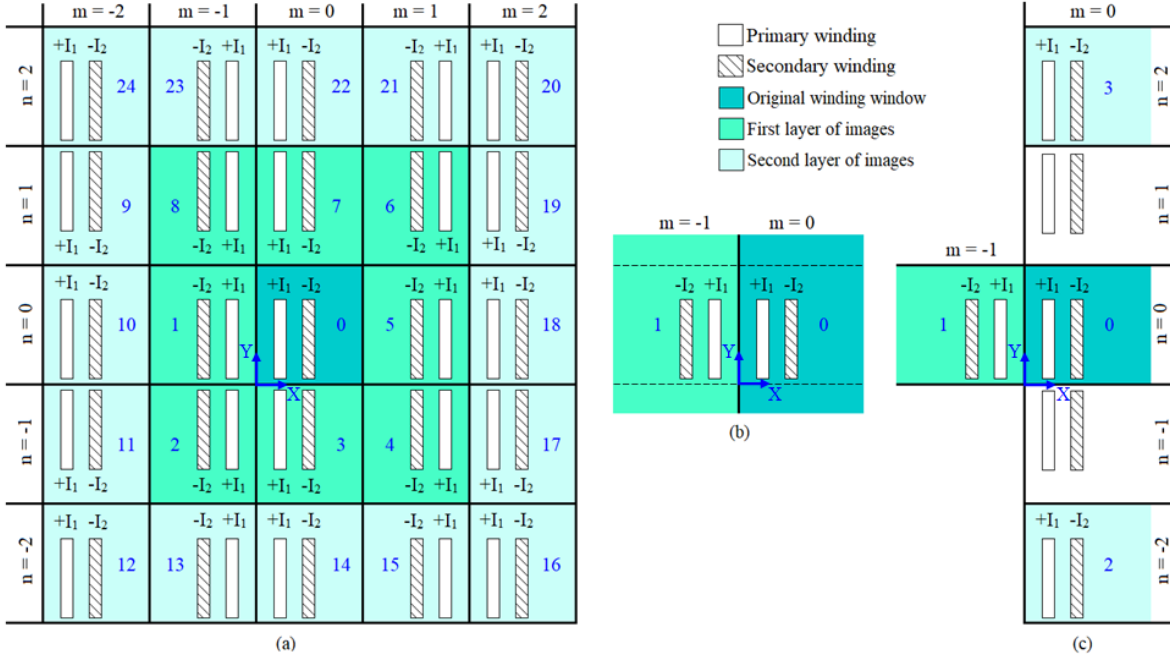


Fig. 3. Image windows resulting from the magnetic image method: (a) IW plane, (b) OW plane, and (c) TR plane.

## II. TRIPLE-2D MODEL

Calculation of leakage inductance is a 3D problem. The Triple-2D model proposed in this paper reduces this 3D problem into three separate 2D problems using the assumption that the leakage inductances per unit length across the IW, OW and TR planes are constant throughout their respective partial leakage lengths. In this paper, the IW plane refers to the rectangular finite plane bounded by the core on all four sides that bisects the volume inside the winding window of the transformer; the OW plane refers to the semi-infinite plane outside the window that is perpendicular to the previous plane at the center of the circular core leg around which concentric windings are wound; and the TR plane refers to the semi-infinite plane located within the transition region, as indicated in Fig. 1. The general form of the proposed Triple-2D model is given by,

$$L_{lk, \text{Triple-2D}} = s_c (L'_{2D(IW)} d_{l(IW)} + L'_{2D(OW)} d_{l(OW)} + 2L'_{2D(TR)} d_{l(TR)}) \quad (1)$$

$$s_c = \begin{cases} 1, & \text{core-type transformer} \\ 2, & \text{shell-type transformer} \end{cases}$$

where,  $L'_{2D(IW)}$ ,  $L'_{2D(OW)}$  and  $L'_{2D(TR)}$  are the leakage inductances per unit length across the IW, OW and TR planes, and  $d_{l(IW)}$ ,  $d_{l(OW)}$  and  $d_{l(TR)}$  are the partial leakage lengths across the IW, OW and TR regions, respectively. Methods to calculate these leakage inductances per unit length and partial leakage lengths are discussed below.

### A. Calculation of Leakage Inductances per Unit Length

The magnetic image method is frequently used in 2D models to calculate the leakage inductance per unit length across a plane. According to the image method, the core acts as a reflective medium for any current-carrying conductor placed

near it. If  $I$  is the current through the actual conductor, then the current through the image conductor  $I_{\text{image}}$  is given by,

$$I_{\text{image}} = \frac{\mu_{r,c} - 1}{\mu_{r,c} + 1} I \quad (2)$$

where,  $\mu_{r,c}$  is the relative permeability of the core. Medium and high-frequency power converters use highly-permeable ferrite cores that have  $\mu_{r,c} \geq 1000$ , so that  $I_{\text{image}} \cong I$ . Details of the image method can be found in [27]. In this paper, image method is used to calculate the leakage inductances per unit length across various planes.

As shown in Fig. 2 (a), the IW plane is bounded by the core on four sides. These four sides act as two pairs of reflective media (mirrors) for a single conductor located in this plane, theoretically resulting in an infinite number of image conductors in both  $x$  and  $y$  directions, as illustrated in Fig. 3 (a). The image locations can be determined following [11]. Since the direction of current in the actual conductor is perpendicular to the plane under consideration, the direction of current in all image conductors will be the same, unlike the incorrect assumption in [19], [20]. At any point  $P(x, y)$  in the IW plane, the total field intensity  $\vec{H}_P^k$  in  $k$  direction due to a single conductor and its images is given by,

$$\vec{H}_P^k(x, y) = \sum_{j=-n}^{+n} \sum_{i=-m}^{+m} \vec{H}_{P(i,j)}^k(x, y) \quad (3)$$

where,  $m \rightarrow \infty$ ,  $n \rightarrow \infty$ ,  $\vec{H}_{P(i,j)}^k$  is the field intensity at  $P(x, y)$  due to a conductor in the  $(i, j)^{\text{th}}$  window,  $i = j = 0$  represents the original window, and  $k$  is either  $x$  or  $y$  direction.

As shown in Fig. 2 (b), the OW plane is bounded by the reflective core on one side only. According to the image method, a single conductor located in this plane yields one image conductor only, as illustrated in Fig. 3 (b). At any point  $Q(x, y)$  in the OW plane, the field intensity  $\vec{H}_Q^k$  in  $k$  direction due to a single conductor and its image is given by,

$$\vec{H}_Q^k(x, y) = \vec{H}_{Q(\text{original})}^k(x, y) + \vec{H}_{Q(\text{image})}^k(x, y) \quad (4)$$

As shown in Fig. 2 (c), the semi-infinite TR plane is bounded by the core on three sides. First, the reflective central core leg yields one image conductor for a single conductor located in this plane. Second, the upper and lower core yokes act as a pair of reflective media. If these core yokes extend to infinity, then an infinite number of image conductors will result along the  $y$  direction. However, they do not extend to infinity, rather they shrink in size along the transition region and are only slightly wider than the winding width. Hence, the leakage energy is not completely bounded by the core yokes along  $y$  direction. The same can also be judged by comparing the three FEM plots of Fig. 2, where the core yokes in the TR plane reduce the magnetic energy density considerably in their neighborhood. This leads to a tricky approximation when applying the image method. Since the image conductors are located directly above or below the actual conductors, their contribution to the total leakage inductance per unit length is always positive. In this paper, the effect of the shrinking core yokes on the total leakage inductance per unit length is approximated by ignoring the contributions of the two closest image windows along  $y$  direction, while adding the contributions of all other image conductors, as illustrated in Fig. 3 (c). Therefore, at any point  $R(x, y)$  in the TR plane, the field intensity  $\vec{H}_R^k$  in  $k$  direction due to a single conductor and its images is given by,

$$\vec{H}_R^k(x, y) = \vec{H}_{R(\text{image})}^k(x, y) + \sum_{j=-n}^{+n} \vec{H}_{R(j)}^k(x, y) \quad (5)$$

where,  $n \rightarrow \infty$ ,  $n \neq 1$ ,  $\vec{H}_{R(j)}^k$  is the field intensity at  $R(x, y)$  due to a conductor in the  $j^{\text{th}}$  window, and  $j = 0$  represents the original window. It should be noted that there would be an infinite series of images along  $m = -1$  that are not shown in Fig. 3 (c). These images contribute negligibly to the total leakage inductance per unit length across the TR plane, and hence are ignored to reduce the computational time.

The total field intensities in  $x$  and  $y$  directions due to all conductors and their respective images are calculated across each plane using,

$$\vec{H}_{P(\text{all})}^k(x, y) = \sum_{\text{all}} \vec{H}_P^k(x, y) \quad (6)$$

$$\vec{H}_{Q(\text{all})}^k(x, y) = \sum_{\text{all}} \vec{H}_Q^k(x, y) \quad (7)$$

$$\vec{H}_{R(\text{all})}^k(x, y) = \sum_{\text{all}} \vec{H}_R^k(x, y) \quad (8)$$

$$H_{P(\text{all})}^2(x, y) = \left( \vec{H}_{P(\text{all})}^{k=x}(x, y) \right)^2 + \left( \vec{H}_{P(\text{all})}^{k=y}(x, y) \right)^2 \quad (9)$$

$$H_{Q(\text{all})}^2(x, y) = \left( \vec{H}_{Q(\text{all})}^{k=x}(x, y) \right)^2 + \left( \vec{H}_{Q(\text{all})}^{k=y}(x, y) \right)^2 \quad (10)$$

$$H_{R(\text{all})}^2(x, y) = \left( \vec{H}_{R(\text{all})}^{k=x}(x, y) \right)^2 + \left( \vec{H}_{R(\text{all})}^{k=y}(x, y) \right)^2 \quad (11)$$

By setting perfectly opposed MMFs in the two windings, the leakage energies per unit length are calculated using,

$$E'_{2D(IW)} = \frac{1}{2} \mu_0 \int_0^h \int_0^w H_{P(\text{all})}^2(x, y) dx dy \quad (12)$$

$$E'_{2D(OW)} = \frac{1}{2} \mu_0 \int_{-\infty}^{\infty} \int_0^{\infty} H_{Q(\text{all})}^2(x, y) dx dy \quad (13)$$

$$E'_{2D(TR)} = \frac{1}{2} \mu_0 \int_0^h \int_0^{\infty} H_{R(\text{all})}^2(x, y) dx dy \quad (14)$$

where,  $w$  and  $h$  are the width and height of the winding window. The coordinate system for each plane is specified in Fig. 3. The improper integrals of (13) and (14) can be solved by assuming the transformer to be located inside an air cube whose sides are longer than the width and height of the transformer.

Assuming the primary current to be  $I$ , the leakage inductance per unit length across each plane is calculated using,

$$L'_{2D(IW)} = \frac{2E'_{2D(IW)}}{I^2} \quad (15)$$

$$L'_{2D(OW)} = \frac{2E'_{2D(OW)}}{I^2} \quad (16)$$

$$L'_{2D(TR)} = \frac{2E'_{2D(TR)}}{I^2} \quad (17)$$

### B. Calculation of Partial Leakage Length

The partial leakage lengths are functions of the magnetic energy distributions across each plane [28]. First, the energy-weighted leakage radius for each plane is calculated using,

$$l_{(IW)} = r_c + \frac{\int_0^h \int_0^w x H_{P(\text{all})}^2(x, y) dx dy}{\int_0^h \int_0^w H_{P(\text{all})}^2(x, y) dx dy} \quad (18)$$

$$l_{(OW)} = r_c + \frac{\int_{-\infty}^{\infty} \int_0^{\infty} x H_{Q(\text{all})}^2(x, y) dx dy}{\int_{-\infty}^{\infty} \int_0^{\infty} H_{Q(\text{all})}^2(x, y) dx dy} \quad (19)$$

$$l_{(TR)} = r_c + \frac{\int_0^h \int_0^{\infty} x H_{R(\text{all})}^2(x, y) dx dy}{\int_0^h \int_0^{\infty} H_{R(\text{all})}^2(x, y) dx dy} \quad (20)$$

where,  $r_c$  is the radius of the circular central core leg around which concentric windings are wound. Although  $l_{(IW)} \approx l_{(OW)} \approx l_{(TR)}$ , they must be evaluated individually for best results. For a circular core leg wound with concentric windings, the partial leakage lengths are also circular, as shown in Fig. 1. These circular leakage lengths are obtained by rotating each plane around the center of the central core leg within their respective regions. The leakage angles in radians subtended at the center of the central core leg (EC-type core) by the three regions of the Triple-2D model are calculated using,

$$\theta_{(IW)} = 2 \arcsin \left( \frac{r_c}{w+r_c} \right) \quad (21)$$

$$\theta_{(TR)} = \arcsin \left( \frac{r_c}{l_{(TR)}} \right) - \frac{\theta_{(IW)}}{2} \quad (22)$$

$$\theta_{(OW)} = \frac{2\pi - s_c(\theta_{(IW)} + 2\theta_{(TR)})}{s_c} \quad (23)$$

For cores not having a circular winding leg, (21) – (23) will change. The leakage radii and the leakage angles at the center of the central core leg are shown in Fig. 1. Finally, the partial leakage lengths are calculated for each region using,

$$d_{l(IW)} = l_{(IW)} \theta_{(IW)} \quad (24)$$

$$d_{l(OW)} = l_{(OW)} \theta_{(OW)} \quad (25)$$

$$d_{l(TR)} = l_{(TR)} \theta_{(TR)} \quad (26)$$

## III. DOUBLE-2D MODEL

The Double-2D model calculates the total leakage inductance of a transformer from the leakage inductances per unit length evaluated across two planes: the IW plane and the

OW plane. The model benefits from the assumption that the evaluated leakage inductances per unit length are consistent along their respective leakage lengths. The general form of the Double-2D model is given by [28],

$$L_{lk, \text{Double-2D}} = s_c (L'_{2D(\text{IW})} d_{l(\text{IW})} + L'_{2D(\text{OW})} d_{l(\text{OW})}) \quad (27)$$

The Double-2D model presented in this paper is deduced from the Triple-2D model discussed above. A similar procedure is followed to calculate  $L'_{2D(\text{IW})}$  and  $L'_{2D(\text{OW})}$ . Since TR regions are not analyzed in the Double-2D model, they are equally divided between the IW and OW regions. From (21), (22) and (23), the leakage angles in radians subtended at the center of the central core leg by the IW and OW regions of the Double-2D model are calculated following,

$$\alpha_{(\text{IW})} = \theta_{(\text{IW})} + \theta_{(\text{TR})} \quad (28)$$

$$\alpha_{(\text{OW})} = \theta_{(\text{OW})} + \theta_{(\text{TR})} \quad (29)$$

where  $\theta_{(\text{TR})}$  is evaluated by replacing  $l_{(\text{TR})}$  in (22) with  $\frac{l_{(\text{IW})} + l_{(\text{OW})}}{2}$ . The leakage angles  $\alpha_{(\text{IW})}$  and  $\alpha_{(\text{OW})}$  are calculated intuitively in [13], [28]. Since the calculation of partial leakage lengths is an integral part of the Double-2D problem, the Double-2D model used in this paper is new and an improvement of the old models. Finally, the energy-weighted partial leakage lengths are calculated for the IW and OW regions using,

$$d_{l(\text{IW})} = l_{(\text{IW})} \alpha_{(\text{IW})} \quad (30)$$

$$d_{l(\text{OW})} = l_{(\text{OW})} \alpha_{(\text{OW})} \quad (31)$$

#### IV. SINGLE-2D MODEL

A computationally efficient Single-2D model, derived from the Triple-2D model, is proposed in this section. This Single-2D model evaluates the total leakage inductance of the transformer from the leakage inductance per unit length evaluated across the TR plane. The analytical and FEM results in Table II verify that the leakage inductance per unit length across the TR plane lies between the leakage inductances per unit length across the OW and IW planes, i.e.  $L'_{2D(\text{OW})} < L'_{2D(\text{TR})} < L'_{2D(\text{IW})}$ . Besides, analytical evaluation of  $L'_{2D(\text{TR})}$  is computationally more efficient than  $L'_{2D(\text{IW})}$  because the TR plane assumes fewer images than the IW plane.

The general form of the proposed Single-2D model for a shell-type or core-type transformer is given by,

$$L_{lk, \text{Single-2D}} = L'_{2D} d_l \quad (32)$$

where,  $L'_{2D} = L'_{2D(\text{TR})}$  and  $d_l = 2\pi l_{(\text{TR})} \cdot L'_{2D(\text{TR})}$  is calculated using (17), whereas  $l_{(\text{TR})}$  is calculated using (20). Since the TR region was not modeled in previous literature, the Single-2D model proposed in this paper is unique.

#### V. CONDUCTOR MODELS

Rectangular foils, Litz wires, or round conductors are commonly used for winding power electronic transformers. Each of these conductor types has its own mathematical formulations to accurately calculate the magnetic field intensities in and around it, which are discussed below.

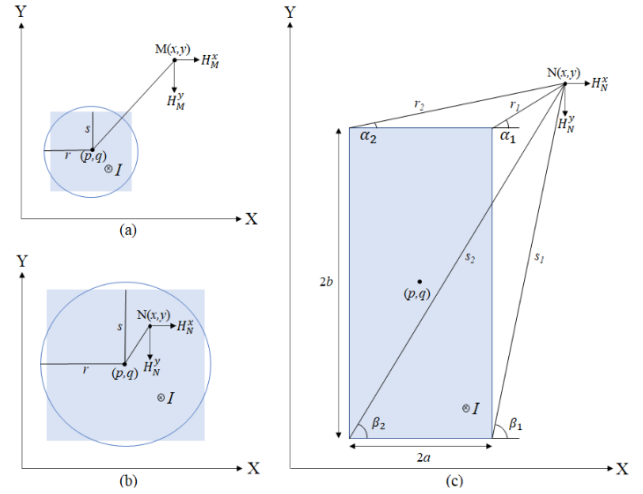


Fig. 4. Conductor models: (a) & (b) round and square conductor, and (c) rectangular foil.

##### A. Round Conductor

Fig. 4 (a) shows a round conductor with radius  $r$  and centered at  $(p, q)$  that is carrying a positive current  $I$ . Using Ampere's law and assuming a homogeneous current density, the magnetic field intensity at  $M(x, y)$  outside the cross-sectional area of the conductor is given by,

$$H_M^x = \frac{I(y-q)}{2\pi[(x-p)^2 + (y-q)^2]} \quad (33)$$

$$H_M^y = \frac{-I(x-p)}{2\pi[(x-p)^2 + (y-q)^2]} \quad (34)$$

With reference to Fig. 4 (b), the field intensity at  $N(x, y)$  inside the cross-sectional area of the conductor is given by,

$$H_N^x = \frac{I(y-q)}{2\pi r^2} \quad (35)$$

$$H_N^y = \frac{-I(x-p)}{2\pi r^2} \quad (36)$$

Two distinct sets of formulations for computing field intensities inside and outside the cross-sectional area of a round conductor increases the complexity of the problem. Although it is easier to compute these field intensities using the polar coordinate system, the winding window, on the other hand, is easier to model using the Cartesian coordinate system. Formulating the entire problem using two coordinate systems makes the analytical calculation of the total leakage inductance very challenging for multiple round conductors. For low-frequency modeling of transformer leakage inductance, a bunch of round-shaped Litz wires can be assumed as a single round conductor having the same current density.

##### B. Square Conductor

To simplify the calculation of field intensities especially inside the cross-sectional area, each round conductor is approximated as a square-shaped conductor having equal cross-sectional area. So, if  $2s$  is the length of one side of a square conductor centered at  $(p, q)$ , then  $s = 0.5 \times \sqrt{\pi r^2}$ . With reference to Fig. 4 (b), the field intensity at  $N(x, y)$  inside the cross-sectional area of the square conductor can be obtained using,

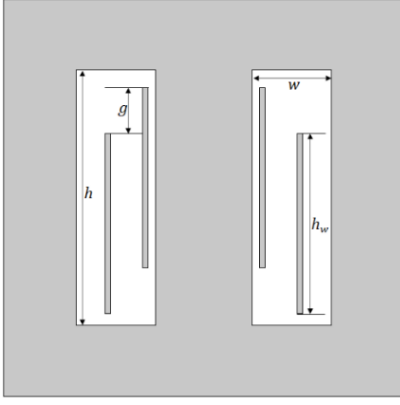


Fig. 5. 2D model of a variable inductance transformer (VIT).

$$H_N^x = \frac{I(y-q)}{8s^2} \quad (37)$$

$$H_N^y = \frac{-I(x-p)}{8s^2} \quad (38)$$

Thus, (37) and (38) replaces (35) and (36). Equations (33) and (34) shall remain valid if appropriate limits for the double integrals are used.

### C. Rectangular foil

With reference to Fig. 4 (c), the magnetic field intensity at any point  $N(x, y)$  for a rectangular foil of height  $2a$  and thickness  $2b$ , whose center is located at  $(p, q)$  is given by [11],

$$H_N^x = \frac{I}{8\pi ab} \left( (y-q+b)(\beta_1 - \beta_2) - (y-q-b)(\alpha_1 - \alpha_2) + (x-p+a) \ln \left( \frac{s_2}{r_2} \right) - (x-p-a) \ln \left( \frac{s_1}{r_1} \right) \right) \quad (39)$$

$$H_N^y = \frac{-I}{8\pi ab} \left( (x-p+a)(\beta_2 - \alpha_2) - (x-p-a)(\beta_1 - \alpha_1) + (y-q+b) \ln \left( \frac{s_2}{s_1} \right) - (y-q-b) \ln \left( \frac{r_2}{r_1} \right) \right) \quad (40)$$

Equations (39) and (40) can calculate the field intensities both inside and outside the cross-sectional area of the foil. However,  $\alpha_1, \alpha_2, \beta_1, \beta_2$  must be strictly maintained within  $(-\pi, \pi)$  range.

Most of the previous literature assumes a layer of round conductors or Litz wires as a single rectangular foil that generates the same MMF when energized with the same current [11], [29]. This assumption introduces errors in the calculation of leakage inductance if the round conductors or Litz wires are not densely packed along the winding height. Assumption of a particular foil thickness can further intensify the error. In this paper, two distinct foil thicknesses are considered: 1) thickness equal to the diameter of a round conductor, and 2) thickness equal to one side of an equivalent square conductor, i.e.  $2s$ , as defined in section V. B. Leakage inductance resulting from the two models are compared in the results section.

## VI. VARIABLE INDUCTANCE TRANSFORMER

An experimental transformer designed for an isolated power converter can exhibit a leakage inductance different from the desired value, often due to geometrical reasons beyond the

TABLE I  
DESIGN SPECIFICATIONS

Description	Value
Core type and size (part)	EC 70 (EPCOS B66343)
Winding height	31.5 mm
External diameter of narrow bobbin	19 mm
External diameter of wide bobbin	32.5 mm
Thickness of the bobbins	1.5 mm
Turns ratio	1:1
Number of turns	26
Primary current	1 A
Maximum change in overlap	10 mm
Conductor shape/size	Round, 19 AWG
Air cube	80 <sup>3</sup> mm <sup>3</sup>

control of the designer. In a power converter system comprising of multiple isolated converters in parallel, all leakage inductances should match to achieve the desired power flow from source to load.

Having a winding height smaller than the window height can allow designers to adjust the leakage inductance of the transformer by moving one of the windings vertically along the core leg, which changes the stored leakage energy between the two windings, and hence the leakage inductance. To achieve a gradual variation of the leakage inductance, a variable inductance transformer (VIT) [30] is introduced and illustrated in Fig. 5, where  $h_w < h$ . By utilizing a linear actuator, one of the two windings can be displaced vertically to vary  $g$ , and consequently the transformer leakage inductance. The leakage inductance is minimum at  $g = 0$  mm, and it increases with  $g$ .

## VII. RESULTS

Design specifications of the shell-type transformer assumed for this work are presented in Table I. The three conductor models considered in this paper are: 1) square conductor, 2) rectangular foil having a thickness equal to the diameter of a round conductor, named as rectangular foil 1, and 3) rectangular foil having a thickness equal to one side of a square conductor, named as rectangular foil 2. Analytical and FEM simulated results of the proposed Triple-2D, Double-2D, and Single-2D models are presented in Tables II, III, and IV, respectively.

For a specific conductor model, the analytically evaluated and FEM simulated values of  $L'_{2D(IW)}$  and  $L'_{2D(OW)}$  in Table II are identical to those in Table III. The same is true for the analytically evaluated and FEM simulated values of  $L'_{2D(TR)}$  in Tables II and IV. Hence, the leakage radii are also equal (not shown in the tables). However, the partial leakage lengths are distinct, because each 2D model assumes different leakage angles at the center of the central core leg for calculating the partial leakage lengths.

### A. FEM Results

A 3D transformer model is designed in COMSOL Multiphysics 5.5 by following the specifications of Table I. Round conductors are used for winding the transformer. To obtain the partial leakage lengths presented in Tables II, III, and IV, three cut planes are created as part of the geometry along the directions indicated by blue lines in Fig. 1 (a) such that the mesh nodes are exactly on the planes. This reduces the 3D FEM

TABLE II  
TRIPLE-2D RESULTS

Conductor model	Category of results	$L'_{2D(IW)}$ (uH/m)	$L'_{2D(TR)}$ (uH/m)	$L'_{2D(OW)}$ (uH/m)	$d_{l(IW)}$ (mm)	$2d_{l(TR)}$ (mm)	$d_{l(OW)}$ (mm)	$L_{lk}$ (μH)	Error (%)
Square conductor	Analytical	154.07	153.6	153.11	10.296	7.987	23.499	12.822	0.02
Rectangular foil 1*	Analytical	152.37	152.21	151.64	10.316	7.941	23.471	12.679	- 1.10
Rectangular foil 2**	Analytical	153.27	153.11	152.54	10.316	7.94	23.473	12.755	- 0.51
Round conductor	3D FEM	-	-	-	-	-	-	12.82	0
	2D FEM***	157.96	155.65	151.75	10.271	7.918	23.366	12.801	- 0.15

TABLE III  
DOUBLE-2D RESULTS

Conductor model	Category of results	$L'_{2D(IW)}$ (uH/m)	$L'_{2D(OW)}$ (uH/m)	$d_{l(IW)}$ (mm)	$d_{l(OW)}$ (mm)	$L_{lk}$ (μH)	Error (%)
Square conductor	Analytical	154.07	153.11	14.263	27.551	12.832	0.09
Rectangular foil 1*	Analytical	152.37	151.64	14.266	27.493	12.685	- 1.05
Rectangular foil 2**	Analytical	153.27	152.54	14.266	27.494	12.761	- 0.46
Round conductor	3D FEM	-	-	-	-	12.82	0
	2D FEM***	157.96	151.75	14.26	27.272	12.782	- 0.30

TABLE IV  
SINGLE-2D RESULTS

Conductor model	Category of results	$L'_{2D} = L'_{2D(TR)}$ (uH/m)	$d_l$ (mm)	$L_{lk}$ (μH)	Error (%)	Computation time (p.u.)
Square conductor	Analytical	153.6	83.366	12.805	- 0.12	0.62
Rectangular foil 1*	Analytical	152.21	83.235	12.669	- 1.18	1
Rectangular foil 2**	Analytical	153.11	83.239	12.745	- 0.58	1
Round conductor	3D FEM	-	-	12.82	0	> 6000
	2D FEM***	155.65	83.373	12.977	1.22	

\* Rectangular foil 1 has a thickness equal to the diameter of a round conductor.

\*\* Rectangular foil 2 has a thickness equal to one side of a square conductor.

\*\*\* Please see subsection A (FEM Results) of section VII (Results) for reference.

model into multiple 2D FEM models that are used for comparison and verification of the three analytical 2D models proposed in this paper.

The leakage inductances per unit length and the leakage radii across each cut plane are obtained using the surface integration tool in COMSOL. The leakage angles and the partial leakage lengths are calculated using the equations presented for different 2D models. The 3D FEM simulated leakage inductance is considered as standard for comparing the analytical model errors in Tables II, III, and IV.

To analyze the TR region further, 7 cut planes are created within the TR region such that the angle between two consecutive cut planes is  $\theta_{(TR)}/6$ . Fig. 6 plots the individual leakage inductances per unit length across each plane. Plane number 1 and 7 are the boundary planes that the TR region shares with the IW and OW regions, respectively. Throughout the TR region, the values of the leakage inductance per unit length showed a maximum variation of about 1 %. Besides, all values lie between those across the IW and OW planes. This confirms that an analysis of the TR plane is necessary for higher accuracy. Since plane number 4 lies at the center of the TR region, the leakage inductance per unit length across this plane, marked in Fig. 6, is used for the 2D FEM results of Tables II

and IV. In Tables II, III, and IV, the error between the 3D FEM simulated and 2D FEM calculated leakage inductances is the lowest for the Triple-2D model, which further proves the hypothesis about the existence of the TR region and validates the formulations for the leakage angles.

### B. Analytical Results

The Triple-2D, Double-2D, and Single-2D models proposed in this paper are used to analytically evaluate the leakage inductance of the shell-type transformer considering the three different conductor models stated in section VII. MATLAB R2019a is used to obtain the analytical results presented in Tables II, III and IV.

For any 2D model, accurate evaluation of the total leakage inductance depends on the accurate evaluation of the leakage inductances per unit length across each plane as well as the partial leakage lengths. Fig. 7 shows the contributions of various image windows along y-direction towards the leakage inductance per unit length across the TR plane. The first stacked graph includes the contribution of the two closest image windows leading to a much higher leakage inductance per unit length when compared to that across the IW plane. This cannot be true because the leakage inductance per unit length across

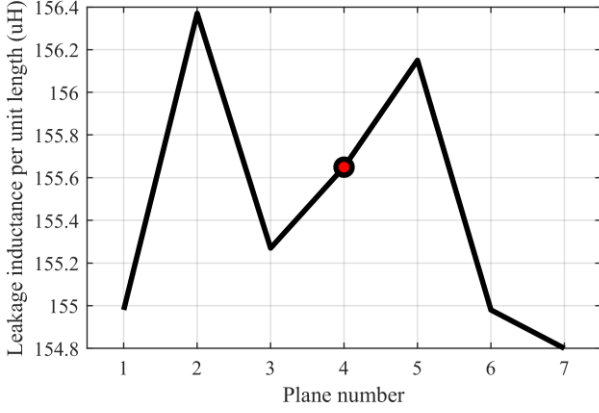


Fig. 6. Plot showing the leakage inductance per unit length across 7 different planes covering the TR region that are obtained from FEM simulations.

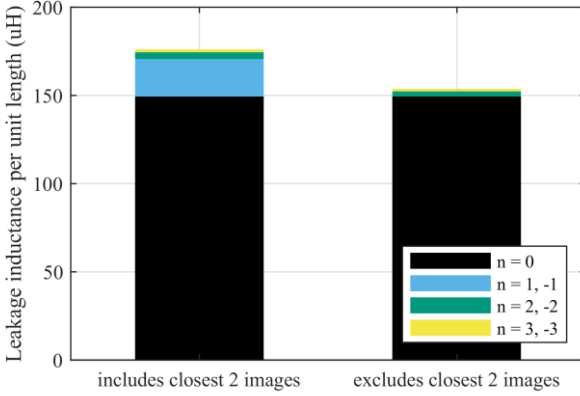


Fig. 7. Contributions of various image windows along y-direction to the leakage inductance per unit length across the TR plane.

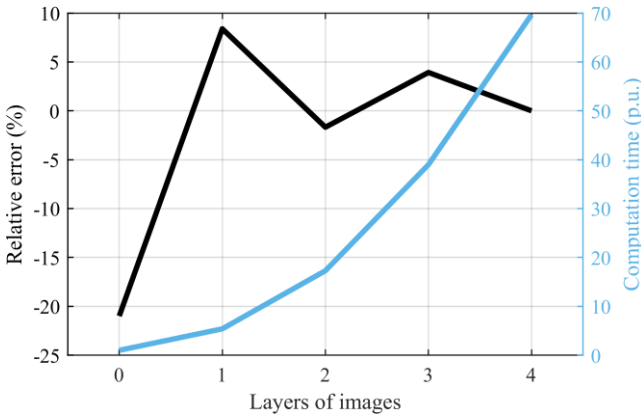


Fig. 8. Plot showing the relative error and computation time for calculating the leakage inductance inside the IW region as the layers of images in the IW plane is increased.

the IW plane should be the highest for a conventional transformer geometry, like the one assumed for this work. The second stacked graph excludes the contributions of the two closest image windows, thus resulting in an acceptable value of the leakage inductance per unit length.

Fig. 8 plots the relative errors in computing the leakage inductance inside the IW region ( $L_{lk,IW\text{-region}} = L'_{2D(IW)} d_{l(IW)}$ )

and the corresponding increase in computation time as the layers of images in the IW plane is increased. A maximum of four layers are considered, i.e. the nearest 80 images, and the leakage inductance due to all four layers is considered as standard for evaluating the relative errors. The computation times in Fig. 8 are represented using the per unit (p.u.) system, where time taken to compute the leakage inductance due to the original conductor only is considered as 1 p.u. Fig. 8 suggests that the computation time increases exponentially as the layers of images are increased. This is because with the addition of an image layer  $u$ , the number of images increases by  $8u$ . As such, a trade-off must be made between accuracy and computational efficiency. In Fig. 8, the error due to the first two layers of images (nearest 24 images) is small and the corresponding computation time is also less. As such, only the first two layers of images are used to calculate the leakage inductance per unit length and partial leakage length across the IW region in Tables II and III.

With the smallest error between the analytical and 3D FEM results, the square conductor model is the closest approximation of round conductors. This is because the current density in a square conductor is identical to that in a round conductor at low frequency. Among the two rectangular foil models, foil 2 results in a smaller error than foil 1 because the current density in foil 2 is higher than that in foil 1. Fig. 9 plots the errors between the analytically evaluated and FEM simulated values of the leakage radii for various conductor models, evaluated using the Triple-2D model. Fig. 10 plots the errors in calculating the leakage angles across the three regions for different conductor models. For Figs. 9 and 10, results from the round conductor-wound 2D FEM model are taken as reference. In Fig. 10, the errors for the IW plane are zero because  $\theta_{(IW)}$  is constant for a specific geometry. All errors in Figs. 9 and 10 are extremely small, which signify the accurate evaluation of the leakage radii as well as the precise identification of the IW, OW and TR regions. Additionally, these two figures jointly validate the formulations presented for calculating the partial leakage lengths.

Fig. 11 compares the computation times of the proposed Triple-2D, Double-2D and Single-2D models assuming rectangular foils, where the computation time of the Single-2D model is taken as 1 p.u. For the IW plane, only the first two layers of images are considered, while for the TR plane, only the second image layer is considered. Sum of the computation times of the Single-2D and Double-2D models roughly equals the computation time of the Triple-2D model. When compared to the Double-2D model, the Triple-2D model increases the computation time by 16 %, whereas the Single-2D model reduces the same by 84 %. Thus, the Single-2D model can be a good choice for optimization-based design of power converters. Table IV further shows that the square conductor model is computationally more efficient than the rectangular foil model. This is due to the convoluted mathematical equations for calculating the field intensities of the foil model (equations (39) – (40)). Besides, these equations encounter singularities at the vertices of the foils, and the angles in these equations must be maintained within  $(-\pi, \pi)$  range for correct results. Nevertheless, the computational efficiency of the square conductor model may drop if the number of square conductors is in the order of hundreds.

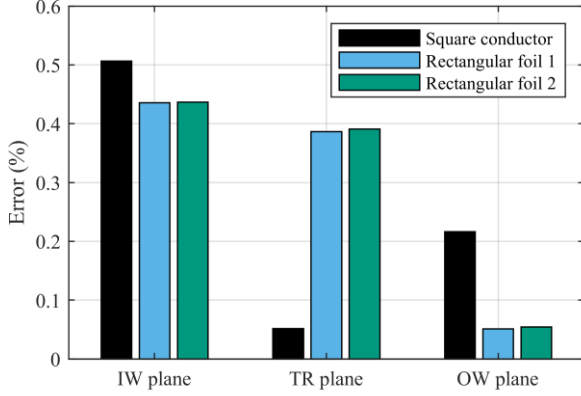


Fig. 9. Errors between the analytically calculated and FEM simulated leakage radii across the three planes for different conductor models evaluated using the Triple-2D model.

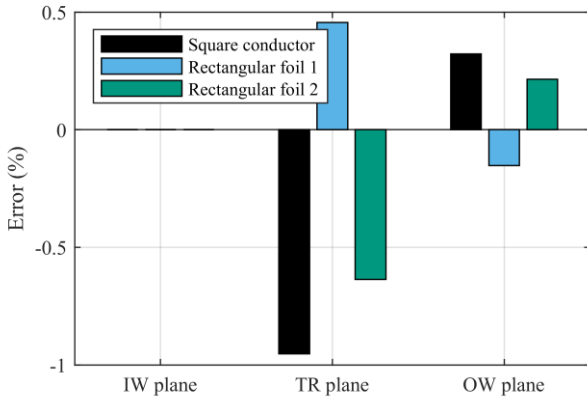


Fig. 10. Errors in calculating the leakage angles across the three regions for different conductor models evaluated using the Triple-2D model.

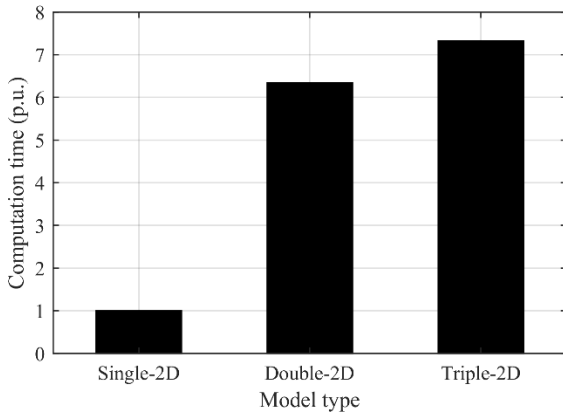


Fig. 11. Relative computation times of the three 2D models proposed in this paper.

### C. Experimental Results

The experimental model of the high-frequency transformer, depicted in Fig. 12, is designed with the specifications presented in Table I. EC 70 cores are used because they have a circular center leg. Perfect round conductors are used to construct the primary and secondary windings. In fact, the experimental model is designed as a variable inductance

transformer, where the narrow bobbin can be moved vertically along the central core leg using a linear actuator to vary  $g$ , and hence the leakage inductance of the transformer.  $g = 0$  mm represents a standard transformer. The leakage inductance of the experimental model at  $g = 0$  mm, measured using an LCR meter at 1 kHz test frequency, is found to be  $13.2 \mu\text{H}$ , which is only 2.96 % higher than the leakage inductance obtained from the FEM model.

### D. VIT Results

The variable leakage inductance of the VIT is modeled analytically as well as in FEM assuming rectangular foil 2. Fig. 13 plots the magnetic energy densities across the IW, OW and TR planes when  $g$  is maximum, i.e.  $g = 10$  mm. When compared to Fig. 2, the energy density is significantly higher in Fig. 13, signifying the increase in leakage inductance when  $g$  is increased from 0 mm to 10 mm. The FEM simulated values of the leakage inductance are in good agreement with the measured values from the experimental prototype for all overlaps, as can be seen from Fig. 14. The leakage inductance of the experimental prototype increased from  $13.2 \mu\text{H}$  at  $g = 0$  mm to  $23.8 \mu\text{H}$  at  $g = 10$  mm.

For analytical modeling, the Double-2D and the Triple-2D models are used to determine the leakage inductance of the VIT at various overlaps  $g$ . First, a Double-2D model with the nearest 2 image layers in the IW plane is used. The resulting errors increase with  $g$ . Next, a Double-2D model with the nearest 3 image layers in the IW plane is used. The errors decreased significantly; the highest error of 4.5 % is observed at  $g = 10$  mm. This suggests that for unsymmetric winding structures, where the centers of the windings do not share the same horizontal plane (e.g. Fig. 5), more image layers may be necessary for better accuracy. Finally, a Triple-2D model with 3 image layers in the IW and TR planes is used. The resulting errors are slightly higher, but quite similar to those obtained using the Double-2D model with the nearest 3 image layers. In fact, the leakage inductance calculated using the Triple-2D model for various conductor types in Table II is also slightly lower than that calculated using the Double-2D model in Table III. A similar difference can be observed between the two plots in Fig. 14.

The Single-2D model may not necessarily result in a better accuracy in case of the VIT because unlike at  $g = 0$  mm, where  $L'_{2D(TR)}$  is approximately the average of  $L'_{2D(IW)}$  and  $L'_{2D(OW)}$  (Table II), at  $g = 10$  mm,  $L'_{2D(TR)}$  is much higher than the average of  $L'_{2D(IW)}$  and  $L'_{2D(OW)}$ , as can be understood from Fig. 13. The Single-2D model may not yield such a high value of  $L'_{2D(TR)}$ , which can lead to a lower overall leakage inductance. Therefore, the proposed Single-2D model is constrained to symmetrical winding geometries, where the windings have the same height and are placed on the same horizontal plane above the lower yoke. However, symmetrical winding is still the most popular choice in transformers, where the proposed Single-2D model can be an excellent trade-off between accuracy and computation time.

## VIII. DISCUSSION

Following are some of the key observations.

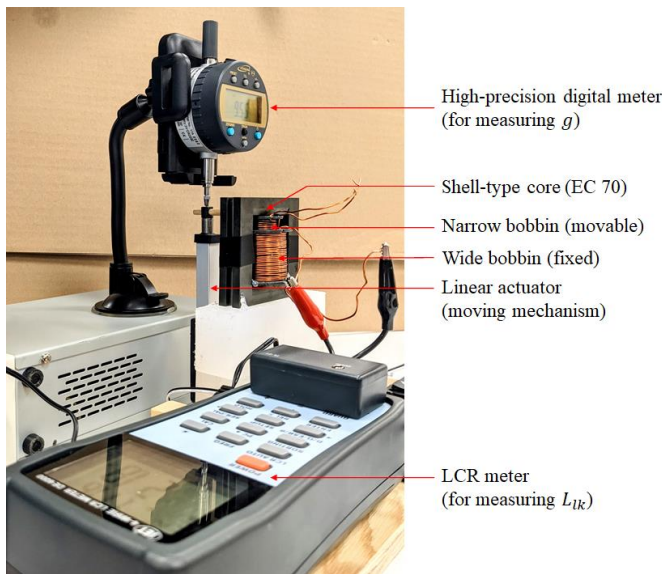


Fig. 12. Experimental prototype of the transformer/VIT.

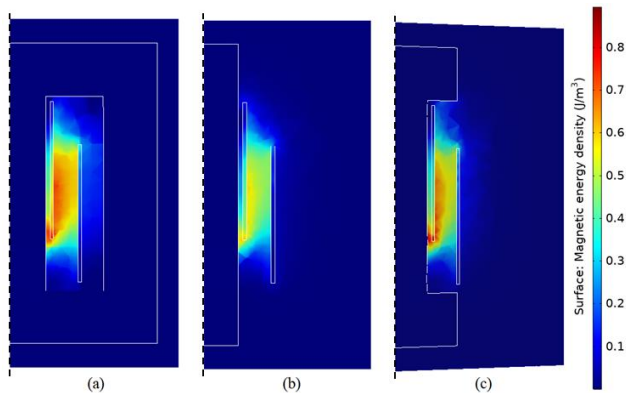


Fig. 13. Magnetic energy densities at  $g = 10$  mm obtained from the 3D FEM model: (a) IW plane, and (b) OW plane, (c) TR plane.

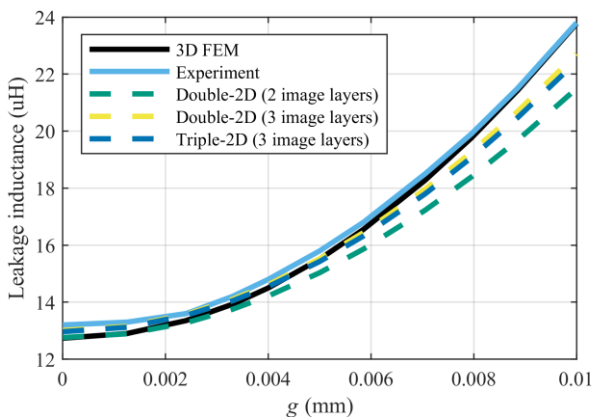


Fig. 14. Plot showing the variable leakage inductance of the VIT at various overlaps,  $g$ .

1) *Triple-2D model*: To model the effect of the shrinking core yokes in the TR region, the contributions of the two closest image windows along  $y$  direction are ignored. The resulting  $L'_{2D(TR)}$  lies between  $L'_{2D(IW)}$  and  $L'_{2D(OW)}$ , which validates the analysis of the TR region. Moreover, accurate

analytical evaluation of the partial leakage lengths highlights the precise identification of the IW, OW and TR regions as well as the accurate calculation of the leakage radii. The Triple-2D model demonstrates the highest accuracy among all three analytical models and is the closest approximation of the 3D transformer geometry.

2) *Double-2D model*: The Double-2D model presented in this paper is a simplification of the Triple-2D model, in which the TR region is equally split between the IW and OW regions. Overall, the Double-2D model is slightly faster than the Triple-2D model because the TR region is not analyzed here. The resulting loss in accuracy or gain in computational efficiency is marginal. The model takes fewer assumptions; hence it should work well for most transformer geometries.

3) *Single-2D model*: Since  $L'_{2D(IW)} > L'_{2D(TR)} > L'_{2D(OW)}$ ,  $L'_{2D(TR)}$  is used to propose the Single-2D model. Because the model is a drastic simplification of the Triple-2D model with much fewer images to account for, its accuracy is compromised. However, the difference in errors is marginal—less than 1%. Moreover, the model demonstrated the least computation time among all three 2D models. Therefore, it can be inferred that the Single-2D model can be an effective tool for evaluating the leakage inductance of a transformer in a multi-objective optimization-based design of isolated power converters. However, the transformer should have a symmetric structure, i.e. the windings should have the same height and they should share the same horizontal base.

4) *Conductor models*: Perfect round conductors are difficult to model. As such, the round conductors used for winding the FEM model and the experimental prototype are assumed as square-shaped conductors in the analytical models, where the cross-sectional area of a square-shaped conductor is equal to that of a round conductor in order to maintain the same current density. Among the three conductor types, the square conductor is the closest approximation of a round conductor because the model results in a similar leakage inductance as the actual round conductors used in the FEM model. Between the two rectangular foil models, the one having a thickness equal to one side of a square conductor results in a lower error than the other because of higher current density. Although square conductors require less computation time than rectangular foils, windings containing multiple layers of square conductors can be quite cumbersome to model.

5) *VIT*: The variable leakage inductance of the VIT is evaluated using the Double-2D and Triple-2D models. Results show that the accuracy is higher for three image layers compared to two image layers in the IW plane. The Triple-2D model with three image layers in the IW and TR planes resulted in errors similar to those obtained using the Double-2D model with three image layers. There exists a small error at higher  $g$  values for both models. The error may be less for multilayer un-interleaved windings. The leakage inductance of the experimental prototype increased from  $13.2 \mu\text{H}$  at  $g = 0$  mm to  $23.8 \mu\text{H}$  at  $g = 10$  mm.

## IX. CONCLUSION

This paper introduces a Triple-2D model that can accurately calculate the leakage inductance of a power electronic transformer with circular center leg from the leakage inductances per unit length evaluated across the IW, OW, and TR planes, and the energy-weighted partial leakage lengths evaluated across the IW, OW, and TR regions. Magnetic image method is used to formulate the Triple-2D model, which can be modified into a Double-2D model by splitting the TR region equally between the IW and OW regions. Since the leakage inductance per unit length across the TR plane lies between those across the IW and OW planes, a unique Single-2D model is proposed, which evaluates the total leakage inductance from the leakage inductance per unit length calculated across the TR plane. This Single-2D model reduces the computation time by more than 84 % when compared to the Double-2D model; therefore, it can be an excellent tool for evaluating the leakage inductance of a symmetrically wound transformer in a multi-objective optimization-based design of isolated power converters. Moreover, all three analytical models exhibit negligible computation errors at  $g = 0$  mm. The proposed models can also be extended to transformer cores with non-circular winding legs, where the equations for calculating the leakage inductances per unit length will remain valid, but the equations for calculating the partial leakage lengths will change depending on the geometry of the windings and the winding leg.

Three different conductor models are analyzed in this paper. Although a square conductor is a close approximation of the actual round conductors used for winding the experimental prototype and requires less computation time than a rectangular foil, it may be difficult to model for a transformer wound with multilayer windings comprising hundreds of round conductors. Rectangular foils are comparatively easier to model, and they present a smaller error when the foil thickness is assumed equal to one side of a square conductor.

The shell-type transformer assumed for validating the proposed 2D models has a partially filled winding window, and the winding height is significantly smaller than the window height. A variable inductance transformer (VIT) is introduced, whose leakage inductance can be varied by moving one of the windings vertically along the central core leg. An experimental prototype of the VIT is designed using a linear actuator. The measured leakage inductances closely follow the FEM simulated values. The Double-2D model used for analytically calculating the leakage inductance of the VIT showed a maximum error of 4.5 % at  $g = 10$  mm.

## ACKNOWLEDGMENT

This material is based upon work supported by the Department of Energy Vehicle Technologies Office under Award Number DE-EE0008449. This report was prepared as an account of work sponsored by an agency of the United States Government. Neither the United States Government nor any agency thereof, nor any of their employees, makes any warranty, express or implied, or assumes any legal liability or responsibility for the accuracy, completeness, or usefulness of any information, apparatus, product, or process disclosed, or represents that its use would not infringe privately owned rights. Reference herein to any specific commercial product,

process, or service by trade name, trademark, manufacturer, or otherwise does not necessarily constitute or imply its endorsement, recommendation, or favoring by the United States Government or any agency thereof. The views and opinions of authors expressed herein do not necessarily state or reflect those of the United States Government or any agency thereof.

## REFERENCES

- [1] J. Zhang, X. Huang, X. Wu, and Z. Qian, "A high efficiency flyback converter with new active clamp technique," *IEEE T. Power Electron.*, vol. 25, no. 7, pp. 1775–1785, Jan. 2010.
- [2] D. Leuenberger and J. Biela, "Accurate and computationally efficient modeling of flyback transformer parasitics and their influence on converter losses," in *EPE'15 ECCE-Europe*, Geneva, Switzerland, 2015, pp. 1–10.
- [3] B. R. Lin, H. K. Chiang, C. E. Huang, K. G. Chen, and D. Wang, "Analysis of an active clamp forward converter," in *Proc. PEDS*, Kuala Lumpur, Malaysia, 2005, pp. 140–145.
- [4] Z. Zhang, J. Huang, and Y. Xiao, "GaN-based 1-MHz partial parallel dual active bridge converter with integrated magnetics," *IEEE T. Ind. Electron.*, 2020. DOI: 10.1109/TIE.2020.3007078.
- [5] M. Stojadinović and J. Biela, "Modeling and design of a medium-frequency transformer for high-power DC-DC converters," *IEEE J. Ind. Appl.*, vol. 8, no. 4, pp. 685–693, Jul. 2019.
- [6] G. Liu, D. Li, Y. Jang, and J. Zhang, "Over 300kHz GaN device based resonant bidirectional DCDC converter with integrated magnetics," in *Proc. APEC*, Long Beach, CA, 2016, 2016, pp. 595–600.
- [7] Y. Zhang, D. Xu, K. Mino, and K. Sasagawa, "1MHz-1kW LLC resonant converter with integrated magnetics," in *Proc. APEC*, Anaheim, CA, 2007, pp. 955–961.
- [8] S. De Simone, C. Adragna, and C. Spini, "Design guideline for magnetic integration in LLC resonant converters," in *SPEEDAM*, Ischia, Italy, 2008, pp. 950–957.
- [9] J. M. Choi, B. J. Byen, Y. J. Lee, D. H. Han, H. S. Kho, and G. H. Choe, "Design of leakage inductance in resonant dc-dc converter for electric vehicle charger," *IEEE Trans. Magn.*, vol. 48, no. 11, pp. 4417–4420, 2012.
- [10] A. Sharma and S. Sharma, "Review of power electronics in vehicle-to-grid systems," *J. Energy Storage*, vol. 21, pp. 337–361, 2019.
- [11] A. Fouineau, M. A. Raulet, B. Lefebvre, N. Burais, and F. Sixdenier, "Semi-analytical methods for calculation of leakage inductance and frequency-dependent resistance of windings in transformers," *IEEE Trans. Magn.*, vol. 54, no. 10, pp. 1–10, 2018.
- [12] M. Nazmunnahar, S. Simizu, P. R. Ohodnicki, S. Bhattacharya, and M. E. McHenry, "Finite-element analysis modeling of high-frequency single-phase transformers enabled by metal amorphous nanocomposites and calculation of leakage inductance for different winding topologies," *IEEE Trans. Magn.*, vol. 55, no. 7, 2019.
- [13] A. F. Hoke and C. R. Sullivan, "An improved two-dimensional numerical modeling method for E-core transformers," in *Proc. APEC*, Dallas, TX, 2002, pp. 151–157.
- [14] J. Zhang, Z. Ouyang, M. C. Duffy, M. A. E. Andersen, and W. G. Hurley, "Leakage inductance calculation for planar transformers with a magnetic shunt," *IEEE Trans. Ind. Appl.*, vol. 50, no. 6, pp. 4107–4112, 2014.
- [15] A. Garcia-Bediaga, I. Villar, A. Rujas, L. Mir, and A. Rufer, "Multiobjective optimization of medium-frequency transformers for isolated soft-switching converters using a genetic algorithm," *IEEE Trans. Power Electron.*, vol. 32, no. 4, pp. 2995–3006, 2017.
- [16] R. Schlesinger and J. Biela, "Comparison of analytical models of transformer leakage inductance: Accuracy versus computational effort," *IEEE Trans. Power Electron.*, vol. 36, no. 1, pp. 146–156, 2021.
- [17] A. K. Das, Z. Wei, S. Cao, S. Vaisambhayana, H. Tian, A. Tripathi, and P. C. Kjær, "Accurate calculation of leakage inductance for balanced and fractional-interleaved winding in medium-frequency high-power transformer," in *Proc. SPEC*, Puerto Varas, Chile, 2017, pp. 1–6.
- [18] Z. Ouyang, O. C. Thomsen, and M. A. E. Andersen, "The analysis and comparison of leakage inductance in different winding arrangements for planar transformer," in *Proc. PEDS*, Taipei, Taiwan, 2009, pp. 1143–1148.
- [19] P. Gómez and F. de León, "Accurate and efficient computation of the inductance matrix of transformer windings for the simulation of very fast transients," *IEEE Trans. Power Del.*, vol. 26, no. 3, pp. 1423–1431, 2011.

- [20] M. Eslamian and B. Vahidi, "New methods for computation of the inductance matrix of transformer windings for very fast transients studies," *IEEE Trans. Power Del.*, vol. 27, no. 4, pp. 2326–2333, 2012.
- [21] M. Lambert, F. Sirois, M. Martinez-Duro, and J. Mahseredjian, "Analytical calculation of leakage inductance for low-frequency transformer modeling," *IEEE Trans. Power Del.*, vol. 28, no. 1, pp. 507–515, 2013.
- [22] C. Wm. T. McLyman, "Winding capacitance and leakage inductance," in *Transformer and Inductor Design Handbook*, 3rd ed., M. O. Thurston, Ed. New York, NY, USA, 2004, pp. 449–460.
- [23] X. Margueron, J. P. Keradec, and D. Magot, "Analytical calculation of static leakage inductances of HF transformers using PEEC formulas," *IEEE Trans. Ind. Appl.*, vol. 43, no. 4, pp. 884–892, 2007.
- [24] W. Tan, X. Margueron, L. Taylor, and N. Idir, "Leakage inductance analytical calculation for planar components with leakage layers," *IEEE Trans. Power Electron.*, vol. 31, no. 6, pp. 4462–4473, 2016.
- [25] S. Mohsenzade, M. Aghaei, and S. Kaboli, "Leakage inductance calculation of the transformers with disordered windings," *IEEE Trans. Plasma Sci.*, vol. 47, no. 4, pp. 1799–1807, 2019.
- [26] M. Mogorovic and D. Dujic, "100 kW, 10 kHz medium-frequency transformer design optimization and experimental verification," *IEEE Trans. Power Electron.*, vol. 34, no. 2, pp. 1696–1708, 2019.
- [27] P. Hammond, "Electric and magnetic images," in *Proc. IEE-Part C: Monographs*, 1960, vol. 107, no. 12, pp. 306–313.
- [28] R. Schlesinger and J. Biela, "Leakage inductance modelling of transformers: Accurate and fast models to scale the leakage inductance per unit length," in *EPE 2020 ECCE Europe*, Lyon, France, 2020, pp. 1–11.
- [29] V. S. Duppalli and S. Sudhoff, "Computationally efficient leakage inductance calculation for a high-frequency core-type transformer," in *ESTS*, Arlington, VA, 2017, pp. 635–642.
- [30] A. Sharma and J. W. Kimball, "Novel transformer with variable leakage and magnetizing inductances," to be published in *Proc. ECCE*, Vancouver, Canada, 2021.

062-057980). He was the general chair of the IEEE Applied Power Electronics Conference in 2017 and continues to serve on its steering committee.



Angshuman Sharma received the B.E. degree from Jorhat Engineering College, Assam, India in 2012, and the M.E. degree from Assam Engineering College, Assam, India in 2014, both in electrical engineering. He is currently pursuing his Ph.D. degree in electrical engineering at the Department of Electrical and Computer Engineering, Missouri University of Science and Technology, Rolla, MO, USA.

His research interests include design of high-frequency magnetics, and modeling and control of power electronic converters.



Jonathan W. Kimball (M'96—SM'05) received the B.S. degree in electrical and computer engineering from Carnegie Mellon University, Pittsburgh, PA, in 1994, the M.S. degree in electrical engineering from the University of Illinois at Urbana-Champaign (Illinois) in 1996, and the Ph.D. degree in electrical and computer engineering from Illinois in 2007.

From 1996 to 1998, he worked for Motorola, Phoenix, AZ, designing IGBT modules for industrial applications. He then joined Baldor Electric, Fort

Smith, AR, where he designed industrial adjustable speed drives ranging 1–150 hp. In 2003, he returned to Illinois as a Research Engineer (later a Senior Research Engineer). Later in 2003, he co-founded SmartSpark Energy Systems, Inc., in Champaign, IL, and served as Vice President of Engineering. He joined the faculty of Missouri S&T (formerly the University of Missouri-Rolla) in 2008 as an Assistant Professor. He was promoted to Associate Professor in 2014 and to Professor of Electrical and Computer Engineering in 2018. From 2016 to 2018, he was also a Dean's Scholar of the College of Engineering and Computing. His research interests include microgrids, switched-capacitor converters, and cyber-physical systems.

Dr. Kimball is a member of Eta Kappa Nu, Tau Beta Pi, and Phi Kappa Phi. He is a Senior Member of the Institute of Electrical and Electronics Engineers (IEEE). He is a licensed Professional Engineer in the State of Illinois (license